ensembles of five forecasts starting from initial conditions corresponding to the 5 days of 26–30 April 1998, and verified during the month of May 1998. Two experiments were run: OSST, with observed SST in 1998; CSST, with climatological SST. To test the effect of the initial conditions an additional ensemble experiment denoted '1993' was run with SST and soil moisture anomalies for 1998, as in OSST, but with initial conditions corresponding to 1993 (a flood year).

Figure 2a shows the observed deficit in precipitation for May 1998, and Fig. 2c shows anomalous low-level moisture transport from the Gulf of Mexico into the Oklahoma–Texas region. They suggest that the drought in May was associated with a lower than normal input of moisture into the region from the low-level jet coming from the Gulf[20,21]. Figure 2b and d show the effect of the SST anomalies present during May. They indicate that the SST anomalies contributed to the establishment of the drought by producing a significant reduction in precipitation, enough to explain about 60% of the deficit observed at that time. Similar experiments were performed for April and June 1998 and the results, summarized in Table 1, generally confirm those obtained for May 1998.

The extent to which the atmospheric conditions in 1998 were already 'primed' to generate the drought is shown in Fig. 3. It is clear that in 1998 the atmospheric circulation would have resulted in lower precipitation than in 1993, even if the surface forcing from SST and soil moisture were the same in both years. The reduction is about 40% of the observed deficit (Table 1).

We tested the second hypothesis (maintenance of the drought through soil-moisture positive feedback) using the regional spectral model. Reanalysis boundary conditions and SSTs were used to drive the RSM during April–September 1998. Only the bottom (deep) soil-moisture model layer was updated from the reanalysis every 24 hours during the model integration period, while the soil moisture in the top (shallow) layer was predicted, to maintain balance with the atmospheric forcing.

Three types of runs were made with the regional spectral model. The first two, CONTROL and CLIMAT, had deep soil moisture replaced by the reanalysis soil moisture for 1998 and the reanalysis 50-year climatology, respectively. As these RSM experiments changed only the lowest soil model layer, they probably underestimated the positive feedback on the drought. To test the effect of a more intense deficit in the soil moisture, we also performed an experiment (DRY) in which the lower-soil model moisture was maintained at the wilting point. The results are presented in Fig. 4. They suggest that soil-moisture anomalies alone would have in fact resulted in an increase in precipitation during April and May, as the early spring had above-normal precipitation and the soil was wetter than normal at the beginning of this period. However, during the summer, soil-moisture feedback could maintain an extreme drought through local feedback. The fact that by September the precipitation recovers to near CLIMAT levels even in the DRY experiment, supports the third hypothesis—that the end of the drought in the autumn was due to stronger events overwhelming the regional positive feedback.

We introduced in this study the use of a regional model nested within the observed large-scale forcing in order to isolate the local feedback mechanism between soil moisture and precipitation. The results suggest that this extratropical climate extreme is not simply rooted in a tropical SST forcing and/or soil-moisture anomalies[2,3,6,7,9,17]. Rather, it is due to a nonlinear coupling of SST anomalies and atmospheric internal forcing organized in the previous months, and a physical interaction with soil-moisture anomalies. At present, statistical seasonal climate predictions are still more skilful than predictions of numerical models[22]. Our results suggest that research with dynamic models, including appropriate physical processes and improved initial conditions, have the potential to overcome this disadvantage. □

Received May; accepted 3 October 2000.

1. Basara, J. B., Arndt, D. S., Johnson, H. L., Brotzge, J. G. & Crawford, K. C. An analysis of the drought of 1998 using the Oklahoma Mesonet. *Eos* **79,** 258 (1998).
2. Bell, G. D. *et al.* Climate assessment for 1998. *Bull. Am. Meteorol. Soc.* **80,** S1–S48 (1999).
3. Barnston, A. G. *et al.* NCEP forecasts of the El Niño of 1997-1998 and its U.S. impacts. *Bull. Am. Meteorol. Soc.* **80,** 1829–1852 (1999).
4. Wallace, J. M. *et al.* On the structure and evolution of ENSO-related climate variability in the tropical Pacific: Lessons from TOGA. *J. Geophys. Res.* **103,** 14241–14259 (1998).
5. Kumar, A. & Hoerling, M. Annual cycle of Pacific-North American predictability associated with different phases of ENSO. *J. Clim.* **11,** 3295–3308 (1998)
6. Atlas, R., Wolfson, N. & Terry, J. The effects of SST and soil moisture anomalies on GLA model simulations of the 1988 US summer drought. *J. Clim.* **6,** 2034–2048 (1993).
7. Wolfson, N., Atlas, R. & Sud, Y. C. Numerical experiments related to the 1980 heat wave. *Mon. Weath. Rev.* **115,** 1345–1357 (1987).
8. Mo, K., Zimmerman, J. R., Kalnay, E. & Kanamitsu, M. A GCM study of the 1988 United States drought. *Mon. Weath. Rev.* **119,** 1512–1532 (1991).
9. Trenberth, K. E., Branstator, G. W. & Arkin, P. A. Origins of the 1988 North American drought. *Science* **242,** 1640–1645 (1988).
10. Shukla, J. & Mintz, Y. The influence of land-surface evaporation on the earth's climate. *Science* **215,** 1498–1500 (1982).
11. Koster, R., Suarez, M. & Heiser, M. Variance and predictability of precipitation at seasonal/to interannual timescales. *J. Hydrometeorol.* **1,** 26–46 (2000).
12. Juang, H.-M. H., Hong, S.-Y. & Kanamitsu, M. The NCEP regional spectral model: An update. *Bull. Amer. Meteorol. Soc.* **78,** 2125–2143 (1997).
13. Roads, J. & Chen, S. Surface water and energy budgets in the NCEP Regional Spectral model. *J. Geophys. Res.* (in the press).
14. Ting, M. & Wang, H. Summertime U.S. precipitation variability and its relation to Pacific sea surface temperature. *J. Clim.* **10,** 1853–1873 (1997).
15. Montroy, D. L. Linear relation of central and eastern North American precipitation to tropical Pacific sea surface temperature anomalies. *J. Clim.* **10,** 531–548 (1997).
16. Montroy, D. L., Richman, M. B. & Lamb, P. Observed nonlinearities of monthly teleconnections between tropical Pacific sea surface temperature anomalies and central and eastern North American prediction. *J. Clim.* **11,** 1812–1835 (1998).
17. Chen, P. & Newman, M. Rossby wave propagation and the rapid development of upper-level anomalous anticyclones during the 1988 US drought. *J. Clim.* **11,** 2491–2504 (1998).
18. Caplan, P. *et al.* Changes to the 1995 NCEP operational medium-range forecast model analysis-forecast system. *Weath. Forecast.* **12,** 581–594 (1997)
19. Kalnay, E. *et al.* The NCEP/NCAR 40-year reanalysis project. *Bull. Am. Meteorol. Soc.* **77,** 437–471 (1996)
20. Bonner, W. D. & Paegle, J. Diurnal variations in the boundary-layer winds over the south central United States in summer. *Mon. Weath. Rev.* **98,** 735–744 (1970)
21. Schubert, S. D., Helfand, H. M., Wu, C.-Y. & Min, W. Subseasonal variations in warm-season moisture transport and precipitation over the central and eastern United States. *J. Clim.* **11,** 2530–2555 (1998).
22. Anderson, J. *et al.* Present-day capabilities of numerical and statistical models for atmospheric extratropical seasonal simulation and prediction. *Bull. Am. Meteorol. Soc.* **80,** 1349–1361 (1999).

Acknowledgements

We thank M. Richman, K. Crawford and J. Basara for helpful discussions.

Correspondence and requests for materials should be addressed to E.K. (e-mail: ekalnay@atmos.umd.edu).

Possible presence of high-pressure ice in cold subducting slabs

Craig R. Bina* & Alexandra Navrotsky†

* *Department of Geological Sciences, Northwestern University, Evanston, Illinois 60208, USA*

† *Thermochemistry Facility, Department of Chemical Engineering and Materials Science, University of California at Davis, Davis, California 95616, USA*

During the subduction of oceanic lithosphere, water is liberated from minerals by progressive dehydration reactions[1,2] and is thought to be critical to several geologically important processes such as island-arc volcanism[3], intermediate-depth seismicity[4] and chemical exchange between the subducting lithosphere and mantle[5]. Although dehydration reactions would yield supercritical fluid water in most slabs, we report here that the stable phase of H_2O should be solid ice VII in portions of the coldest slabs. The formation of ice VII as a dehydration product would affect the generation, storage, transport and release of water in cold sub-

duction zones and equilibrium conditions of dehydration would shift, potentially affecting the depths of seismogenesis and magmagenesis. Large amounts of pure ice VII might accumulate during subduction and, as a sinking slab warms, eventual melting of the ice would release large amounts of water in a small region over a short period of time, with a significant positive volume change. Moreover, the decreasing availability of fluid water, owing to the accumulation of ice VII and its subsequent reaction products in a cooling planetary interior (for example, in Mars or the future Earth), might eventually lead to a decline in tectonic activity or its complete cessation.

Supercritical fluid water is the stable phase of H_2O at high pressure and temperature, but at low temperature the stable high-pressure phase is the cubic (space group *Pn*3*m*) solid ice VII[6,7]. We investigated whether conditions within some subducting lithospheric slabs fall within the ice VII stability field. The recently measured melting curve of ice VII is shown in Fig. 1. Superimposed on this curve are a range of subduction zone thermal models, giving minimum temperatures inside model slabs, together with a mean mantle geotherm. We note that, given the uncertainties in slab thermal models (see Methods), the temperature curves for the cooler families of slabs cross the phase boundary between water and ice VII.

Also shown in Fig. 1 are equilibrium reaction boundaries for three representative dehydration reactions—brucite to periclase[8], lawsonite blueschist to quartz eclogite[9,10] and antigorite (serpentine) to enstatite plus the dense hydrous magnesium silicate 'phase A'[2]. The latter two reactions are believed to be important in terrestrial subduction zones[11,12]. These phase relations for melting and dehydration will also be sensitive to the solubility of solid phases in the aqueous phase. What are the potential effects of forming solid ice VII instead of supercritical fluid water by dehydration during subduction?

One effect of initial dehydration in the stability field of ice VII rather than of water is to change the sign of the Clapeyron slope (dP/dT) of the dehydration reaction, because of the low entropy of ice VII relative to that of water. Thus, the onset of dehydration will be at lower pressures, and hence at shallower depths, in the ice VII stability field. The pressure–temperature (P–T) dehydration curves will be more nearly linear (constant $\Delta S/\Delta V$) when ice rather than fluid is formed, because of the expected smaller compressibility and thermal expansivity of ice. Thus the dehydration reaction will resemble a solid–solid phase transition. The volume change (ΔV) of dehydration becomes significantly more negative (by ~50%) at the onset of ice VII formation; hence a greater reduction in free energy is available for a given pressure overstep of the reaction boundary. This increases the driving force of reaction and may inhibit metastable persistence of the hydrated phase assemblage. On the other hand, the absence of a fluid phase in which the minerals can dissolve may hinder the kinetics of dehydration, which might otherwise occur by a dissolution–reprecipitation mechanism. Moreover, these changes in dP/dT and ΔV reflect a change in sign of the enthalpy of reaction (ΔH), so that the endothermic dehydration reactions become exothermic upon entering the ice VII stability field. Thus the heat balance, driving force, and rates of dehydration are expected to be different when the evolved H_2O is solid.

The release of H_2O as ice VII from hydrous minerals allows its continued transport downward in solid form, rather than its rapid lateral and upward movement as a fluid. The lower mobility and buoyancy of ice VII implies less rapid infiltration and ascent of H_2O, allowing the possibility of later water-consuming reactions, such as the incorporation of H_2O into wadsleyite (β-Mg_2SiO_4)[13] or the formation of dense hydrous magnesium silicates such as phase A[14], if the H_2O released as ice VII continues moving downward with the slab. Furthermore, the absence of fluid water as a solvent implies minimal transport of solutes, such as incompatible elements, as long as H_2O remains crystalline. Thus the H_2O formed as ice VII will not carry the geochemical signature of its initial formation conditions. However, as soon as this ice melts, it will form a corrosive fluid, pure water, which will react rapidly with the rocks where it first forms. The resulting mineral–water equilibrium and geochemical signature will represent the greater depth at which ice VII melted, rather than the range of shallower depths over which dehydration occurred.

The formation of ice VII from hydrous phases will occur gradually[11,14], reflecting multivariant dehydration curves of multicomponent mineral solid solution assemblages, but its later melting to water should be univariant (that of a pure single-component substance), occurring at one specific pressure and temperature as the P–T boundary is crossed. Furthermore, melting of ice VII should be much more rapid than the reconstructive dehydration

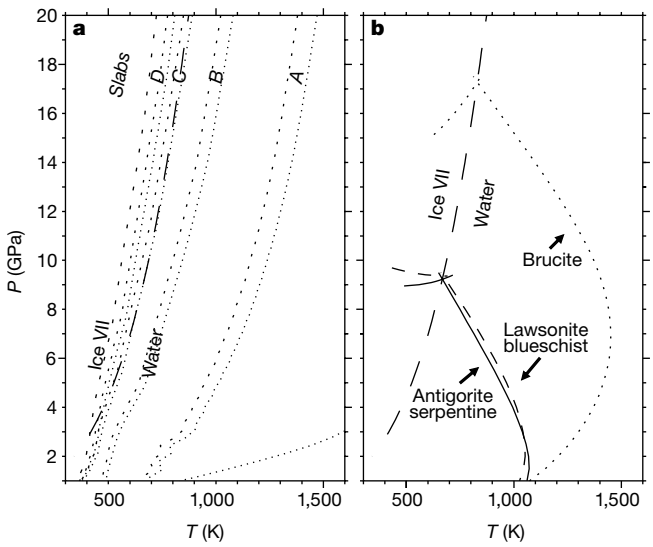

Figure 1 The melting curve of ice VII. Data from experimental measurements of melting conditions[28]. Heavy dashed line shows the melting curve. **a**, Superimposed are the minimum temperatures inside slabs, calculated for a range of subduction zone thermal models (slab classes[19] A, B, C and D) along with a typical mantle geotherm (dotted lines). **b**, Superimposed are calculated equilibrium reaction boundaries for three representative dehydration reactions: brucite to periclase (dotted lines), lawsonite blueschist to quartz eclogite (dashed lines), and antigorite (serpentine) to enstatite plus phase A (solid lines).

of silicate minerals. This implies a sudden release of fluid H_2O when the slab leaves the ice VII stability field. Such sudden, rather than gradual, release of water has important implications for arc volcanism and seismicity. As both arc magmagenesis and intermediate-depth seismogenesis are believed to be H_2O-mediated processes, the depth-distribution of melting and of earthquakes may reflect the availability of water as a function of depth along individual slab geotherms. To estimate the magnitude of these effects, if the hydrated portion of the slab contains about 6 wt% H_2O[14], then about 0.01 mole of H_2O can be liberated per cm^3 of material, corresponding to a volume change of about 1%. The approximately 0.1 cm^3 of water per cm^3 of material thus suddenly liberated is immediately available for melting, the transport of ions and other reactive chemistry.

The presence of solid H_2O within a slab should also perturb other subduction zone properties, particularly if this ice is carried downward until it melts or reacts chemically. Changes in buoyancy and rheology, for example, should arise from the low density and strength, respectively, of ice near its melting point. Aggregate seismic velocities, too, should be affected by the relatively low acoustic velocities in ice VII[15,16]. Although it is perhaps mitigated by the high symmetry of cubic ice VII, the potential for growth of large ice crystals also raises the possibility of observable changes in elastic anisotropy.

The detection of ice VII under conditions of cold subduction is possible by *in situ* (infrared, Raman, synchrotron X-ray) experimental study, as is the potential for transport of H_2O to even greater depths by other higher-pressure ice polymorphs[17]. Quenched metastable ice VII can also be studied (by neutron diffraction) at ambient pressures[18].

Evidence for the geophysical signature of ice VII could be sought, for example, in Tonga, one of the world's coldest subduction zones[19], which also exhibits unusual patterns of seismicity and volcanism. Whereas subduction zone seismicity generally declines with increasing depth, attaining a minimum at 300–400-km depth before rising again, seismicity beneath Tonga exhibits a more marked increase in seismic moment release near 400 km depth than do other subduction zones. If seismicity at and above such depths is related to water, as is commonly asserted[4,19], then perhaps significantly greater amounts of water become available near this depth beneath Tonga than elsewhere. Furthermore, slow seismic velocity anomalies extend to 400 km beneath the Tonga volcanic arc and the adjacent Lau back-arc basin, suggesting that partial melting related to the release of volatiles from the slab may occur near this depth[20]. If water is transported by ice VII beneath Tonga, then the ice may melt near this depth, providing water in a concentrated dose. Indeed, although the thermal models in Fig. 1 show the lowest temperatures in the slab at any depth, actual isotherms will migrate into the slab's interior as the slab surface warms with increasing depth, so that P–T paths followed by individual particles will have shallower slopes than depicted. Given the uncertainties in both the Tonga slab geotherm (class D in Fig. 1) and the ice VII melting curve, ice VII formed by dehydration near 150 km, for example, should melt somewhere in the 300–800-km depth interval. Thus, melting near 13 GPa (400 km) is possible. Furthermore, this pressure is near that at which wadsleyite becomes stable, so any released H_2O could potentially affect the α–β phase transition in olivine and thus the properties of the 410-km seismic discontinuity[1].

Of course, the dehydration of real multicomponent mineral phases produces an aqueous fluid containing dissolved ionic species. These dissolved species affect both the equilibrium dehydration curves and the ice melting equilibria; both are depressed in temperature. Thus, the extent to which a given local geotherm enters the ice VII field may be modified from that presented in a simple calculation, but the balance between the formation of solid ice by dehydration and the formation of an aqueous fluid will be affected less strongly than either reaction (ice melting and ordinary dehydration) alone. The arguments presented above, and especially those for cooler planetary regimes (see below) remain valid, although the exact locations of phase boundaries will be affected. Indeed, owing to the low temperatures and the large latent heat of fusion for ice VII, reducing the fluid activity from unity to 0.9 should result in a melting-point depression of order 1–10 K over the pressure range 0–20 GPa.

Finally, the role of ice phases in subduction should assume a growing importance as a planet cools through geologic time. As its average geotherm becomes cooler, it is reasonable to expect that, if plate tectonics or a similar process is occurring, a growing fraction of subducting slabs will contain regions of ice VII stability. Thus, the phenomena discussed above will grow more important as a planet cools and should be considered in models of future Earth evolution. Ice VII may be even more important in the martian interior. Although the temperature distribution within Mars is poorly constrained, the planet's smaller size lends it a much faster cooling rate[21], so that the interior should be colder than Earth's[22]. Any past episodes of subduction should have efficiently cooled the martian interior and effectively transported surface water (by a thick hydrothermally altered crust) to the deep mantle[21], whereas the fraction of subducting slabs in the stability field of ice VII should have been much greater than on Earth. As a planet cools so that its normal geotherm approaches the ice VII field, progressively less subducted water may be returned to the surface; it will instead be stored in ice and/or hydrous mineral phases in the slabs. With less water, volcanism will diminish, breaking the plate tectonic cycle. Hence, growing transport of H_2O to the deep interior as ice VII and subsequent storage in a reservoir of ice or hydrous mineral phases may have served to deprive Mars of its earlier surface water, to limit deep melting, and to end (or considerably slow) martian plate tectonics. It has been suggested that late Tharsis volcanism on Mars may have involved deep H_2O release attributable to later radioactive heating[21]. Although the magnitude of radioactive heating is even more poorly constrained for the interiors of other planets than it is for Earth's, such late release of water is consistent with either ice VII melting or dehydration upon local reheating.

Thus, water initially present in planetary oceans becomes trapped in sediments, subducted and immobilized in the deep interior. Accumulation of ice VII or its by-product hydrous phases may eventually lead to a tectonically dead planet with a dry surface. Planetary bodies and their satellites in solar and extrasolar planetary systems are strikingly diverse, and understanding the origins and consequences of such variability is a major goal of planetary science. We suggest that the state (fluid versus crystalline) of H_2O in planetary interiors can profoundly affect both dynamics and thermal balance, and that changes in the relative proportions of fluid and solid H_2O can alter the subsequent evolution of a planetary body. Perhaps the presence or absence of ice VII in planetary interiors, like that of ice I on planetary surfaces, is one of the important factors influencing the different possible paths of planetary evolution. □

Methods

Calculation of subduction zone thermal models yields a range of possible slab geotherms, depending upon the various assumptions and parameters employed. The purpose of our calculations is not to argue for one model in preference to another but simply to generate a suite of reasonable temperature profiles. If a significant number of these intersect the melting curve of ice VII, then the main hypothesis of this Letter is supported. We computed subduction zone thermal models using a standard kinematic finite-difference method[23] for four thermal classes[19] of slabs. Class A represents young slabs (age is 12 Myr, rate is 6 cm yr^{-1}, dip is 30°; for example, Cascadia, Mexico, Nankai Trough), class B represents middle-aged slabs (50 Myr, 7 cm yr^{-1}, 45°; for example, Middle America, northern Chile, central Aleutians), class C represents old slabs (140 Myr, 8 cm yr^{-1}, 60°; for example, eastern Indonesian, Kuriles), and class D represents old and rapidly subducting slabs (140 Myr, 14 cm yr^{-1}, 60°; for example, Tonga). To illustrate a range of thermal profiles (Fig. 1), for each class of slab we first computed thermal structures for a plate model with a high (1,450 °C, ref. 24, fine dotted curves) basal lithospheric temperature, thereby reproducing the published models for these four thermal classes[19]. We then recomputed thermal structures for the same plate models but with a moderate (1,325 °C, ref.

25, medium dotted curves) basal lithospheric temperature. Finally, for the coldest class, D, we also computed a thermal structure for a halfspace model with a moderate (1,325 °C, ref. 25, heavy dotted curve) basal temperature. These simple models neglect both shear and radiogenic heating, effects which would raise slab temperatures. However, we also neglect additional effects which would lower slab temperatures. In northern Tonga, for example, rates can reach 24 cm yr^{-1}, ref. 26), thus preserving colder slab temperatures to great depths. Moreover, the fixed kinematic slab boundaries of our simple model do not allow for the thermal insulation effect of the viscous blanket that develops on a slab's upper surface in a mantle with temperature-dependent viscosity, an effect which further depresses slab temperatures at depth in more sophisticated models of dynamically evolving slabs[27].

We used the melting curve of ice VII as determined from contrasting indices of refraction by direct visual observation[28], rather than from earlier studies based on the disappearance of diffraction peaks that provided only lower bounds on melting points[6]. From this curve, we used thermodynamic equations of state for water[8] and ice VII[6,29] to calculate a best-fit specific heat function and enthalpy and entropy values for ice VII, obtaining parameters ($\Delta H = -290.3$ kJ mol^{-1}, $S^0 = 41.46$ J K^{-1} mol^{-1}, $C_p = 59.91$ J K^{-1} $mol^{-1} + 2.904 \times 10^{-3}\,T - 1.509 \times 10^{+6}\,T^{-2}$) in reasonable agreement with those derived from earlier melting curves[6]. We then used these thermodynamic parameters to calculate equilibrium reaction boundaries for three representative dehydration reactions (brucite to periclase[8], lawsonite blueschist to quartz eclogite[9,10], and antigorite (serpentine) to enstatite plus the dense hydrous magnesium silicate 'phase A'[2]), in both the water and ice VII stability fields, using the equations of a state for antigorite[2], brucite[30], phase A[31], and the set of minerals periclase, glaucophane, lawsonite, jadeite, diopside, pyrope, quartz and enstatite[32].

Received 9 May; accepted 12 September 2000.

1. Wood, B. J., Pawley, A. & Frost, D. R. Water and carbon in the Earth's mantle. *Phil. Trans. R. Soc. Lond. A* **354,** 1495–1511 (1996).
2. Bose, K. & Navrotsky, A. Thermochemistry and phase equilibria of hydrous phases in the system MgO-SiO_2-H_2O: Implications for volatile transport to the mantle. *J. Geophys. Res.* **103,** 9713–9719 (1998).
3. Hirschmann, M. M., Asimov, P. D., Ghiorso, M. S. & Stolper, E. M. Calculation of peridotite partial melting from thermodynamic models of minerals and melts. III. Controls on isobaric melt production and the effect of water on melt production. *J. Petrol.* **40,** 831–851 (1999).
4. Green, H. W. II & Houston, H. The mechanics of deep earthquakes. *Annu. Rev. Earth Planet. Sci.* **23,** 169–213 (1995).
5. Regelous, M., Collerson, K., Ewart, A. & Wendt, J. I. Trace element transport rates in subduction zones: Evidence from Th, Sr, Pb isotope data for Tonga-Kermadec lavas. *Earth Planet. Sci. Lett.* **150,** 291–302 (1997).
6. Fei, Y., Mao, H.-K. & Hemley, R. J. Thermal expansivity, bulk modulus, and melting curve of H_2O-ice VII to 20 GPa. *J. Chem. Phys.* **99,** 5369–5373 (1993).
7. Wolanin, E. *et al.* Equation of state of ice VII up to 106 GPa. *Phys. Rev. B* **56,** 5781–5785 (1997).
8. Belonoshko, A. & Saxena, S. K. A molecular dynamics study of the pressure-volume-temperature properties of super-critical fluids: I. H_2O. *Geochim. Cosmochim. Acta* **55,** 381–387 (1991).
9. Peacock, S. M. The importance of blueschist → eclogite dehydration reactions in subducting oceanic crust. *Geol. Soc. Am. Bull.* **105,** 684–694 (1993).
10. Helffrich, G. in *Subduction Top to Bottom, Geophysical Monograph 96* (eds Bebout, G. E., Scholl, D. W., Kirby, S. H. & Platt, J. P.) 215–222 (American Geophysical Union, Washington DC, 1996).
11. Ono, S. Stability limits of hydrous minerals in sediment and mid-ocean ridge basalt compositions: Implications for water transport in subduction zones. *J. Geophys. Res.* **103,** 18253–18267 (1998).
12. Iwamori, H. Transportation of H_2O and melting in subduction zones. *Earth Planet. Sci. Lett.* **160,** 65–80 (1998).
13. Smyth, J. R. A crystallographic model for hydrous wadsleyite ($\beta - Mg_2SiO_4$): An ocean in the Earth's interior? *Am. Mineral.* **79,** 1021–1024 (1994).
14. Schmidt, M. W. & Poli, S. Experimentally based water budgets for dehydrating slabs and consequences for arc magma generation. *Earth Planet. Sci. Lett.* **163,** 361–379 (1998).
15. Baer, B. J., Brown, J. M., Zaug, J. M., Schiferl, D. & Chronister, E. L. Impulsive stimulated scattering in ice VI and ice VII. *J. Chem. Phys.* **108,** 4540–4544 (1998).
16. Shimizu, H., Nabetani, T., Nishiba, T. & Sasaki, S. High-pressure elastic properties of the VI and VII phase of ice in dense H_2O and D_2O. *Phys. Rev. B* **53,** 6107–6110 (1996).
17. Goncharov, A. F., Struzhkin, V. V., Mao, H. & Hemley, R. J. Raman spectroscopy of dense H_2O and the transition to symmetric hydrogen bonds. *Phys. Rev. Lett.* **83,** 1998–2001 (1999).
18. Klotz, S. *et al.* Metastable ice VII at low temperature and ambient pressure. *Nature* **398,** 681–684 (1999).
19. Kirby, S. H., Stein, S., Okal, E. A. & Rubie, D. C. Metastable mantle phase transformations and deep earthquakes in subducting oceanic lithosphere. *Rev. Geophys.* **34,** 261–306 (1996).
20. Zhao, D. *et al.* Depth extent of the Lau back-arc spreading center and its relation to subduction processes. *Science* **278,** 254–257 (1997).
21. Sleep, N. H. Martian plate tectonics. *J. Geophys. Res.* **99,** 5639–5655 (1994).
22. Sohl, F. & Spohn, T. The interior structure of Mars: Implications from SNC meteorites. *J. Geophys. Res.* **102,** 1613–1635 (1997).
23. Toksöz, M. N., Sleep, N. H. & Smith, A. T. Evolution of the downgoing lithosphere and the mechanisms of deep focus earthquakes. *Geophys. J. R. Astron. Soc.* **35,** 285–310 (1973).
24. Stein, C. A. & Stein, S. A model for the global variation in oceanic depth and heat flow with lithospheric age. *Nature* **359,** 123–129 (1992).
25. Davies, J. H. & Stevenson, D. J. Physical model of source region of subduction zone volcanics. *J. Geophys. Res.* **97,** 2037–2070 (1992).
26. Bevis, M. *et al.* Geodetic observations of very rapid convergence and back-arc extension at the Tonga arc. *Nature* **374,** 249–251 (1995).
27. Kincaid, C. & Sacks, I. S. Thermal and dynamical evolution of the upper mantle in subduction zones. *J. Geophys. Res.* **102,** 12295–12315 (1997).
28. Datchi, F., Loubeyre, P. & LeToullec, R. Extended and accurate determination of the melting curves of argon, helium, ice (H_2O), and hydrogen (H_2). *Phys. Rev. B* **61,** 6535–6546 (2000).
29. Loubeyre, P., LeToullec, R., Wolanin, E., Hanfland, M. & Hausermann, D. Modulated phases and proton centring in ice observed by X-ray diffraction up to 170 GPa. *Nature* **397,** 503–506 (1999).
30. Robie, R. A. & Hemingway, B. S. Thermodynamic properties of minerals and related substances at 298.15 K and 1 bar (10^5 pascals) pressure and at higher temperatures. *US Geol. Surv. Bull.* **2131,** 1–461 (1995).
31. Pawley, A. R. & Wood, B. J. The low-pressure stability of phase A, $Mg_7Si_2O_8(OH)_6$. *Contrib. Mineral. Petrol.* **124,** 90–97 (1996).
32. Gottschalk, M. Internally consistent thermodynamic data for minerals in the system SiO_2-TiO_2-Al_2O_3-Fe_2O_3-CaO-MgO-FeO-K_2O-Na_2O-H_2O-CO_2. *Eur. J. Mineral.* **9,** 175–223 (1997).

Acknowledgements

We thank R. Hemley and J. Longhi for helpful comments. C.R.B. acknowledges the support of the US National Science Foundation and of the Earthquake Research Institute of the University of Tokyo. A.N. acknowledges the support of the Center for High-Pressure Research, an NSF Science and Technology Center, and of the Kreeger-Wolf Endowment at Northwestern University.

Correspondence and requests for materials should be addressed to C.R.B. (e-mail: craig@earth.northwestern.edu).

Analysis of an evolutionary species–area relationship

Jonathan B. Losos* & Dolph Schluter†

** Department of Biology, Campus Box 1137, Washington University, St. Louis, Missouri 63130, USA*
† Zoology Department and Centre for Biodiversity Research, University of British Columbia, Vancouver, British Columbia V6T IZ4, Canada

Large islands typically have more species than comparable smaller islands. Ecological theories, the most influential being the equilibrium theory of island biogeography[1], explain the species–area relationship as the outcome of the effect of area on immigration and extinction rates. However, these theories do not apply to taxa on land masses, including continents and large islands, that generate most of their species *in situ*. In this case, species–area relationships should be driven by higher speciation rates in larger areas[2–6], a theory that has never been quantitatively tested. Here we show that *Anolis* lizards on Caribbean islands meet several expectations of the evolutionary theory. Within-island speciation exceeds immigration as a source of new species on all islands larger than 3,000 km^2, whereas speciation is rare on smaller islands. Above this threshold island size, the rate of species proliferation increases with island area, a process that results principally from the positive effects of area on speciation rate. Also as expected, the slope of the species–area relationship jumps sharply above the threshold. Although *Anolis* lizards have been present on large Caribbean islands for over 30 million years, there are indications that the current number of species still falls below the speciation–extinction equilibrium.

The 143 species of Caribbean island *Anolis* lizards are ideal for a test of evolutionary theories of diversity. The group has been there since at least the middle Oligocene and has radiated extensively within the archipelago[7–9]. Current species richness on islands is related to area, and both immigration and speciation have contributed[10,11]. We used a phylogeny for Caribbean *Anolis* species based on mitochondrial DNA[9] to estimate the number of immigration and speciation events on islands. By comparing these quantities with island area, we can test three predictions that derive from an evolutionary theory of species–area relationships: (1) a threshold island size should exist, above which speciation surpasses immigration as a source of new species; (2) above the threshold size, recorded speciation events per unit time on the large islands should increase with island area; (3) the slope of the species–area